The performance of a smart ball-and-socket actuator applied to upper-limb rehabilitation

El-Wahed, Ali; Balkhoyor, Loaie

Published in:
Journal of Intelligent Material Systems and Structures

DOI:
10.1177/1045389X18780349

Publication date:
2018

Document Version
Peer reviewed version

This is the accepted manuscript version of the article: The performance of a smart ball-and-socket actuator applied to upper-limb rehabilitation, El-Wahed, A. & Balkhoyor, L. 11 Apr 2018 In : Journal of Intelligent Material Systems and Structures. Link to final version DOI:

The performance of a smart ball-and-socket actuator applied to upper-limb rehabilitation

Ali K. El Wahed* and Loaie B. Balkhoyor

Mechanical Engineering, University of Dundee, Dundee DD1 4HN, United Kingdom

**Corresponding author. Email: a.elwahed@dundee.ac.uk*

ABSTRACT

Magnetorheological (MR) fluids are capable of providing continuously variable yield stresses in response to external magnetic fields. Greater potential application in rehabilitation may be realised if these fluids are utilised in controllable actuators offering multi-degree-of-freedom (MDOF) motions. This paper presents the results of the comparative performance of a ball-and-socket actuator, employing MR fluids as the controllable medium, using theoretical and numerical approaches. The theoretical model combines the viscous-friction and the controllable field-dependent characteristics of the MR fluid in which a Bingham plastic model is used to simulate the shear stress of the fluid under various input conditions. A special procedure to simulate the device performance using computational fluid dynamics (CFD) techniques, which were performed using ANSYS CFX computer code, is detailed. Three commercial MR fluids (MRF241-ES, MRF132-AD, and MRF122-2ED) were assessed and it was found that the simulated values of the device torque compared well with the theoretical values.

Keywords: Magnetorheological fluids, ball-and-socket actuator, CFD simulations.

1. INTRODUCTION

1.1 General Introduction

Strokes occur when the brain does not get enough blood supply, which is due to a blocked artery or an internal bleeding. Although, one-third of the people might survive a stroke, they could be left with control, sensory or cognitive function lost, which depends on the impaired part of the brain (Abrams and Berkow, 1997). One common consequence is the movement and co-ordination of the upper limb, when about 85% of people with stroke show this deficiency (Parker et al., 1986). In addition, comparable injuries such as sports, occupational and spinal cord injuries are considered as common causes of upper limb impairment. Therefore, musculoskeletal disorders are recognised as a major cause of morbidity in the UK, which account for over 15% of all General Practitioner

(GP) consultations (Peters et al., 1984) and 78% of referrals for physiotherapy assessment from GP's (Dundee Healthcare NHS Trust, 1992-1997).

Once the critical stage of the stroke or the spinal injury is over, patients are engaged in an intensive rehabilitation programme, which is designed to suit individual patient condition. The principle aim of the physiotherapist is then to assist in the restoration of the function, which is intrinsically dependent on the presenting limiting factors of pain, loss of movement and muscle weakness. It is well documented that the upper limb is more difficult to recover its functions in comparison with the lower limb impairment extremity. Therefore, several investigators have faced the challenges of upper limb rehabilitation with the use of increased intensity of standard physical therapy treatments (Lincoln et al., 1999), device enhanced treatment (Feys et al., 1998) or neuromuscular stimulation (Powell et al., 1999) for the affected limb.

The death rate from stroke and related diseases is expected to be reduced by 40% by the year 2020, which means up to 200,000 lives will be saved per year (Paterson et al., 2000) leaving the NHS with a huge rehabilitation task. This will add to the 15% well recognised current national shortage of chartered physiotherapists working in the NHS (The Chartered Society of Physiotherapy, 1998). Consequently, initiatives that would allow a more efficient use of existing staffing levels are required, in order to provide direct benefit to the quality of patient care. Mechanical-assisted devices are already in use in physiotherapy, but a new generation of intelligent therapy-assisted machines is needed if there is to be a significant impact on the numbers of patients that can be treated under current staffing level.

1.2 The Programmable Physiotherapy Concept

A multi-degree-of-freedom (MDOF) orthotic arm employing smart actuation technology and a suitable control strategy would be expected to offer a realistic solution to the current physiotherapist shortage in the NHS. These advanced orthotic arms should be provided with the required safety features so that they can work within pre-defined kinematic and force constraints. This means that a physiotherapist should be able to start a specific rehabilitation training programme using one of these programmable systems, leaving the patient to complete the exercise without his/her direct supervision, whilst focusing on other patients who need the most specialised manual attention and hence more patients will be dealt with at the same time. These smart orthoses should also be equipped with a graphical user interface for instructing and guiding patients while they perform their training tasks.

1.3 Upper-Limb Orthotics

The use of robotics for the delivery of upper-limb post-stroke rehabilitation has already been proposed by several research groups. A typical robot-assisted rehabilitation system may consist of servomotors and link mechanisms, which has an impedance control system to ensure the required level of compliance and human safety (Baklouti et al., 2010). A Balanced Forearm Orthosis (BFO) was probably one of the earliest upper-limb orthotics which was developed in 1965 as a passive device to enable a person with weak musculature to move their arms in horizontal planes (Alexander et al., 1992). This orthosis however was rarely used due to problems associated with its gravity compensation. A five degree-of-freedom version of the BFO powered by means of electric motors was then produced in 1975 but this never gained significant acceptance due to the same gravity compensation problem (Stern and Lauko, 1975). A hybrid arm orthosis which takes advantage of a wheelchair frame was developed to provide upper-arm motion assistance (Benjuya and Kenney, 1990), which offered a body-powered shoulder abduction and elbow flexion in addition to a motor-powered wrist supination and a three-joint jaw chuck pinch. Dijkers et al. (1991) used a simple therapy robotic arm offering six DOF motions to study the acceptance of robot technology in occupational therapy by both patients and therapists. Researchers at MIT developed another robot designed for the physical therapy of stroke victims (Krebs et al., 1998), which was able to guide or move patient's upper-limb and can record important data in relation to the position, velocity, and applied forces. Homma and Arai (1995) reported another orthotic device that is attached to a wheelchair, which used a parallel mechanism to permit motions of the upper-limb. Another motorised upper-limb orthoses with a 5 DOF capability (3 DOF at the shoulder, 1 DOF at the elbow and 1 DOF for pronation/supination of the forearm) was developed in the mid-90s (Johnson and Buckley, 1997), but problems associated with its complex safety and control hampered its further development. A device for evaluating arm impairments after brain injury was developed (Reinkensmeyer et al., 1999), which comprised an instrumented linear constraint that could be oriented in different directions across the patient's workspace using a three-splined steel shaft. Scientists at Stanford University developed and clinically tested a mechatronic orthosis for post-stroke therapy (Burgar et al., 2000), which was designed to handle multiple functional movement patterns and to have the capability to fully support the upper-limb during passive and active modes of therapy. A haptic master of 6 DOF (3 translational and 3 rotational DOF) was developed (Hawkins et al., 2002) with the aim to explore and identify best therapies for machine mediated stroke rehabilitation. A seven DOF prototype upper-arm rehabilitation system was reported Tsagarakis and Caldwell, 2003), which utilises pneumatic muscle actuators as power source to generate the required motions. Although the pneumatic actuators have excellent power to weight ratio, a number of them was used to provide the required DOF at each joint of the arm,

which increased the total weight of the uncompensated orthosis. Recently, an upper-limb rehabilitation robot, ARMin, was developed (Nef et al., 2009), which is a four active (three for the shoulder and one for the elbow actuation) and two passive DOF device.

1.4 Smart Fluids

Electrorheological (ER) and magnetorheological (MR) fluids, which belong to the general area of smart materials, can exhibit massive and reversible changes in their rheological properties such as yield stress, when energised by electric and magnetic fields, respectively. Both fluids involve suspensions or slurries of solid particulates, typically micrometres in size, in liquids. Their response to an applied field is the familiar chaining of the particles in the direction of the field and the resulting "solidification" or increase in the apparent viscosity of the fluids. Industrial applications of these fluids, during the last two decades, have seen considerable progress. Vibration control is considered to be the most promising area of the large-scale commercial exploitation of these fluids, which can provide controlled damping forces to meet many industrial requirements (El Wahed and Balkhoyor, 2016). However, some ER fluid devices have failed to meet their design functions, principally because they require fluids with a yield stress that is higher than that currently available. On the other hand, MR fluids have enjoyed a recent surge in their engineering application, due mainly to their high yield stress. As a result, MR fluids have enabled the construction of useful industrial devices, such as automotive shock absorbers, that are impractical to fabricate using ER fluids.

Recently, numerous studies on the design of rotary smart fluid actuators, such as clutches or brakes, have been reported (see for example Nguyen et al., 2015). This is an area of application that has not developed as much as might have been predicted. This is generally ascribed to the inadequate levels of shear yield stress that is required for such applications. However, Kavalicoglu et al. (2008) reported a 43-plate MR fluid clutch that was capable of 244 N.m torque transmission for an input electric current of 3 A.

MR fluids have been used commercially since the mid-1990s. The first application was an MR fluid rotary brake, manufactured by Nautilus, and used in home exercise equipment to provide a programmable resistance (Anon, 1995). Since 1998, semi-active MR actuators have been developed for use in off-road and heavy vehicles (McManus and St. Clair, 2000), forklift vehicles (Linde, 2000), racing vehicles (Arre Industries, 1998) and tractors (Claas Tractor Times, 2008). In 2002, Delphi Corporation developed a semi-active MR fluid shock absorber system (Delphi Energy and Chassis Systems, 2002), which is now available on numerous vehicles including

Cadillac, Chevrolet, Buick, Ferrari, Honda and Audi. Another successful commercial use of this technology is the smart prosthetic knee, which improves the mobility of above-the-knee leg amputees (Carlson et al., 2001). Clearly, commercial MR devices are used widely and new applications are emerging continuously to exploit their inherent characteristics.

1.5 Smart Fluid Actuators in Rehabilitation

To overcome the drawbacks of conventional systems, a few groups attempted to develop ER and MR fluid-based rehabilitation devices. Sakaguchi et al. (1999) developed a force display system using ER actuators, which was equipped with a computer program to evaluate the physical capability of upper limbs of patients. A 3 DOF exercise machine was developed, which can be used as a motion guide robot or a force display device in which ER actuators were incorporated to provide safety during upper-limb physiotherapy exercises (Furusho et al., 2002). A new robot, which consists of two MR fluid clutches, two induction motors and a feedback control system, was proposed for knee-joint rehabilitation (Hakogi et al., 2006). Another rehabilitation device was developed to provide a passive resistance during strength training of muscles (Dong et al., 2006), which employs a programmable axial MR fluid actuator that could apply a resistance as prescribed by a physical therapist. Similarly, rotary MR (Zite et al., 2006) and ER (Nikitczuk et al., 2007) actuators were proposed as controllable knee braces. Furusho et al. (2006) developed a rehabilitation robot which is a 6 DOF (3 DOF for the shoulder and elbow, and the other 3 DOF for the wrist) force display system for upper-limbs when each DOF was realised by ER actuators. A novel one DOF smart hand-interfaced device was developed (Khanicheh et al. (2008) to assess patient's handgrip capability under brain magnetic resonance imaging (MRI). Kikuchi et al. (2009) developed a rehabilitation training system for upper-limbs, which has 2 controllable DOF on the working plane and 1 passive DOF of the inclined angle of the working plane. This system utilises ER actuators for its torque control.

2. MR FLUID BALL-AND-SOCKET ACTUATOR

The human arm can handle a MDOF motions along a multiple-axis system as it benefits from a flexibility offered by joints with a ball-and-socket structure. For example, the arm could be raised above the head, lowered beside the body, extended from the body or moved forward across the body. In addition, the arm rotates in a 360-degree circle when held to the side. Consequently, any developed orthosis aimed for the rehabilitation of human upper-limbs should have similar flexibility at its joints. Currently, rotary MR fluid actuators exist primarily in two different configurations, namely disc-type and cylindrical-type, which permit one DOF movements. As a

result, these actuators are not useful if they are proposed to control the joints of an upper-limb rehabilitation orthotic device. Accordingly, a ball-and-socket configuration has been chosen by the authors to design a novel type of MR actuators (Figure 1a), which has been derived from the structure of the human shoulder joint (Figure 1b).

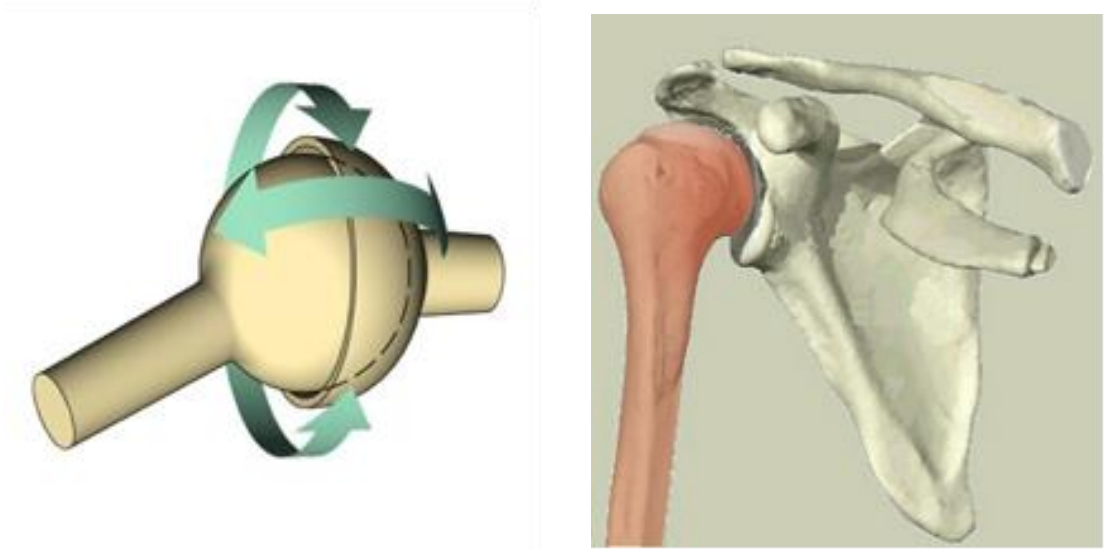

(a) (b)

Figure 1. Ball-and-socket joint (a) mechanical joint, (b) human shoulder joint

This work has been ongoing by the authors since 2009 when ball-and-socket MR actuators have been developed (Trivedi, 2009; Almazroa, 2011) with the aim of their incorporation into rehabilitation orthotic arm joints to give them movement adaptability and controllability similar to those offered by a human upper-limb. The concept of a ball-and-socket joint was investigated several years ago when an electric motor based on this principle was developed to control a three degree-of-freedom motion in a single robot wrist joint (Lee et al., 1996). Also, the application of a spherical brake for haptics was reported earlier (Senkal and Gurocak, 2009). In addition, recent attempts have suggested the use of an electrorheological spherical actuator for applications in robot-assisted cutting surgery (Hwang et al., 2016).

The work reported in this manuscript is focused on the performance of the MR fluid ball-and-socket actuator under various input conditions, which is assessed using theoretical and numerical approaches. The theoretical model utilises a non-Newtonian fluid model whilst ANSYS CFX computational fluid dynamics (CFD) code was used to achieve the numerical results. Advanced

CFX capabilities such as its three-dimensional solid-liquid interaction and non-Newtonian fluid flow analyses were well suited to the present investigation and enabled the calculation of the dynamic properties of the MR fluid, such as the fluid shear stress, when the actuator's ball is subjected to a motion. This allowed the estimation of the device output torque as a function of the magnetic flux density, which was compared well with the results calculated by the theoretical model. A range of commercial MR fluids, manufactured by Lord Corporation, were used in this investigation.

3. THEORETICAL MODELLING OF THE DEVICE TRANSMITTED TORQUE

The work reported in this paper is only focused on the development of a ball-and-socket actuator for the shoulder joint. The human shoulder is capable of providing flexion/extension torques of a peak value of about 110 N.m as well as adduction/abduction torques of a peak value of about 125 N.m (Baklouti et al., 2010). However, shoulder rehabilitation orthoses are usually designed with a torque capability that is well below these peak values, which is normally set at 50 N.m (Dickerson et al., 2006). This is because the output torque is not constant for the whole range of motion and its peak value is only required at specific joint positions (Jaffar et al., 2006). As a result, 50 N.m has been set as target for the torque delivered by the developed ball-and-socket actuator, which is assumed achievable under an induced magnetic flux density generated by the actuator coil in the range of 1.3–1.5. This magnetic flux density range represents the saturation point for most commercial MR fluids (Lord Corporation, 2008). In order to achieve the desired shoulder movements, the ball-and-socket joint has also been designed with an opening angle (from one socket edge to another) of 125°.

Figure 2 shows a schematic representation of the developed ball-and-socket actuator for the purpose of this study. A step-by-step approach was employed in the design process of the developed actuator and its electromagnetic circuit. The electromagnetic coil, which is located inside the socket part of the actuator, consists of 488 turns of 30 AWG wire with 0.3 mm outer diameter and is driven by a maximum current of 2.1 Ampere. Based on the above specifications as well as the cross sectional area of the coil, a current density of 2.277×10^7 Ampere/m^2 was estimated. Further details on the electromagnetic and mechanical design of this actuator will be presented in a separate technical manuscript.

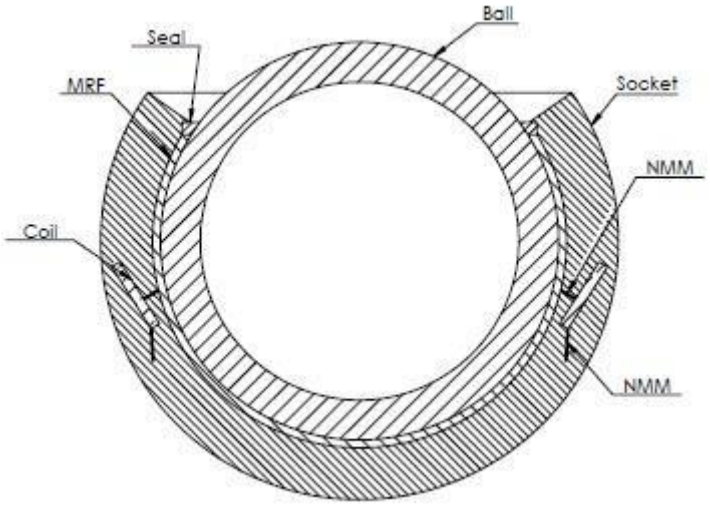

Figure 2. Section view showing the main elements of the ball-and-socket actuator

In order to account for the non-Newtonian behaviour of the MR fluid, the Bingham plastic fluid model (Shames and Cozzarelli, 1992) is utilised, which is the most commonly used model to describe the shear stress of MR fluids:

$$\tau = \eta \dot{\gamma} + \tau_y(H) \tag{1}$$

where τ, $\tau_y(H)$, and η are the shear stress, dynamic yield stress which is dependent on the magnetic field intensity H, and dynamic viscosity of the MR fluid, respectively, whilst $\dot{\gamma}$ is the shear rate. The total torque T_t delivered by the MR ball-and-socket actuator comprises three components. These are the controllable field-dependent torque T_y, the viscous friction torque T_v, and the mechanical friction torque T_m (Almazroa, 2011). Hence, T_t is:

$$T_t = T_y + T_v + T_m \tag{2}$$

In practical applications, the torque due to the mechanical friction T_m, which is mainly caused by mechanical seals, is relatively small compared with the other two torque components. Hence, it could be discarded from the current analysis. Although the majority of the actuator torque comes from the yield stress of the fluid, the torque due to the viscous-friction T_v has been included in this analysis so that the effect of the angular velocity at which the device is utilised as part of the current rehabilitation application is also accommodated.

Since spherical components are involved in this analysis, the Cartesian x and y axes were

identical and therefore, the spherical coordinate system shown in Figure 3 is employed to mathematically derive the torque produced along the three axes (*x*, *y*, *z*).

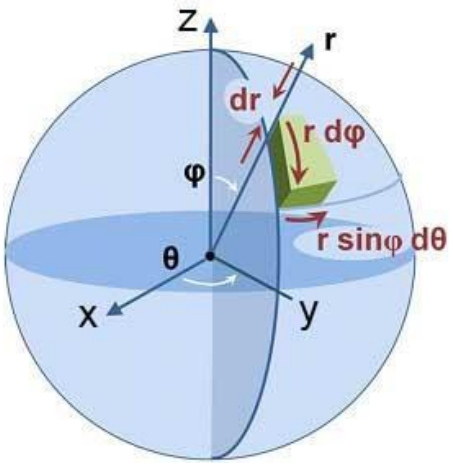

Figure 3. Schematic diagram showing spherical coordinate system

The field-dependent torque T_y is first calculated by integrating a minute torque, which is due to a shear force created by the fluid shear stress acting on an infinitesimally small area *dA* of the actuator ball, over the ball area *A* in contact with the MR fluid, Figure 3:

$$T_y = \iint_A \tau_y(H)\, r_m \, dA \tag{3}$$

where r_m is the moment arm that is given by:

$$r_m = r \sin\varphi \tag{4}$$

The infinitesimal area *dA* is given by

$$dA = r^2 \sin\varphi \, d\varphi \, d\theta \tag{5}$$

Combining equations (3), (4) and (5) yields:

$$T_y = \int_0^{\varphi} \int_0^{2\pi} \tau_y(H)\, r \sin\varphi \, r^2 \sin\varphi \, d\varphi \, d\theta$$

$$\therefore \quad T_y = \tau_y(H)\, r^3 \int_0^{\varphi} \int_0^{2\pi} \sin^2\varphi \, d\varphi \, d\theta \tag{6}$$

The viscous-friction T_v can also be derived following the same philosophy:

$$T_v = \iint_A \eta\, \gamma\, r_m\, dA \tag{7}$$

The shear rate, γ is given as:

$$\gamma = \frac{r_m\, \omega}{h} \tag{8}$$

where ω is the angular velocity and h is the MR fluid gap size.

Using equation (8) and noting that the moment arm r_m and infinitesimal area dA are still given by Eqs. (4) and (5), respectively. Thus, Eq. (7) can be rewritten as:

$$T_v = \int_0^{\varphi} \int_0^{2\pi} \eta\, \frac{r_m\, \omega}{h}\, r \sin\varphi\, r^2 \sin\varphi\, d\varphi\, d\theta$$

which is simplified to yield equation (9) below:

$$T_v = \int_0^{\varphi} \int_0^{2\pi} \eta\, \frac{r \sin\varphi\, \omega}{h}\, r \sin\varphi\, r^2 \sin\varphi\, d\varphi\, d\theta$$

$$T_v = \eta\, \frac{r^4\, \omega}{h} \int_0^{\varphi} \int_0^{2\pi} \sin^3\varphi\, d\varphi\, d\theta \tag{9}$$

Now, equations (2), (6), and (9) are combined to give the total torque T_t:

$$T_t = \tau_y(H)\, r^3 \int_0^{\varphi} \int_0^{2\pi} \sin^2\varphi\, d\varphi\, d\theta + \eta\, \frac{r^4\, \omega}{h} \int_0^{\varphi} \int_0^{2\pi} \sin^3\varphi\, d\varphi\, d\theta \tag{10}$$

Integrating equation (10) yields:

$$T_t = \pi\, r^3\, \tau_y(H)\left(\varphi - \sin\varphi\cos\varphi\right) + \frac{8\,\eta\,\pi\, r^4\, \omega}{3\,h} \sin^4\left(\frac{\varphi}{2}\right)\left(\cos\varphi + 2\right) \tag{11}$$

One water-based (MRF241-ES) and two oil-based (MRF132-AD and MRF122-2ED) commercial

MR fluids, which were manufactured by Lord Corporation, were used in this investigation. The MR fluid yield stress, $\tau_y(H)$ can be calculated as a function of the particle volume fraction, ψ as well as the magnetic field intensity, H using the following empirical equation (Lord Corporation, 2008):

$$\tau_y(H) = C \cdot 2.717.10^5 \cdot \Psi^{1.5239} \cdot Tanh\left(6.33 \cdot 10^{-6} \; H\right) \qquad (12)$$

where C is a constant, which is set to 1 and 1.1253 for oil-based and water-based MR fluids, respectively. Figure 4 shows the calculated yield stresses for MRF241-ES, MRF132-AD, and MRF122-2ED with volume fractions of 41%, 32%, and 22%, respectively, as a function of magnetic field intensities of up to 700 kA/m.

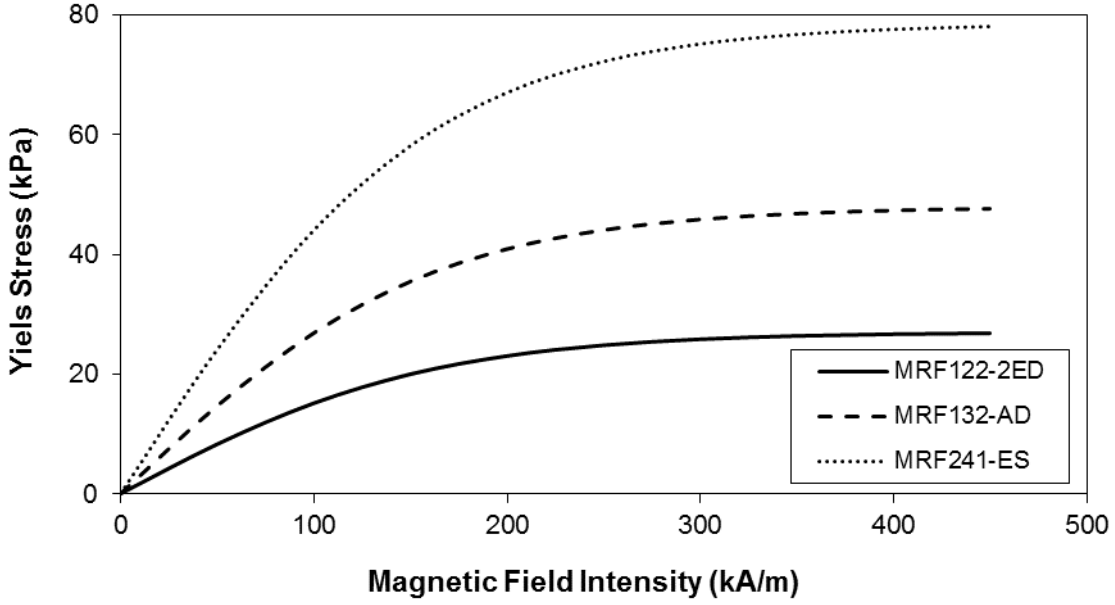

Figure 4. Yield stress versus field intensity for three commercial MR fluids

The relationship between the magnetic flux density B and magnetic field intensity, H for the above three fluids can be estimated using the following empirical equation (Lord Corporation, 2008):

$$B = 1.91 \cdot \Psi^{1.133} \cdot \left[1 - Exp\left(-10.97 \cdot \mu \cdot H\right) + \mu \cdot H\right] \qquad (13)$$

where μ is a magnetic constant which is set to 1.566×10^{-6}. Figure 5 shows the estimated flux densities, for the three commercial MR fluids, as a function of the magnetic field intensity.

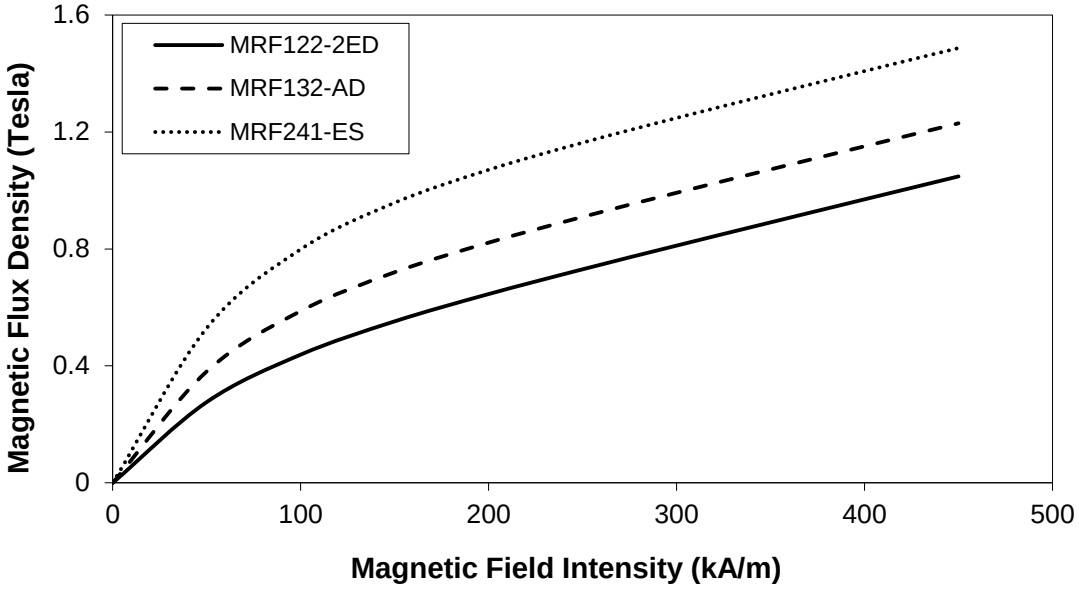

Figure 5. Magnetic flux density versus field intensity for three commercial MR fluids

Table 1 details the above calculated flux densities together with the corresponding yield stresses for the three commercial MR fluids, which are required as inputs for the CFD simulations. This will be detailed later in Section 4.

Table 1 Yield stresses and magnetic flux densities for three commercial MR fluids

Field Intensity (kA/m)	MRF122-2ED		MRF132-AD		MRF241-ES	
	Flux Density (T)	Yield Stress (kPa)	Flux Density (T)	Yield Stress (kPa)	Flux Density (T)	Yield Stress (kPa)
50	0.27	8.28	0.38	14.66	0.52	24.06
100	0.44	15.14	0.58	26.80	0.79	44.00
150	0.55	19.99	0.72	35.39	0.95	58.10
200	0.646	23.05	0.82	40.81	1.07	67
250	0.73	24.84	0.90	43.98	1.16	72.20
300	0.81	25.85	0.99	45.76	1.24	75.12
350	0.89	26.40	1.07	46.73	1.32	76.72
400	0.96	26.70	1.15	47.26	1.40	77.58
450	1.04	26.85	1.22	47.54	1.48	78.04
500	1.12	26.94	1.30	47.69	1.56	78.2
550	1.20	26.98	1.38	47.77	1.64	78.42
600	1.28	27.01	1.46	47.81	1.72	78.49
650	1.36	27.02	1.54	47.83	1.80	78.53
700	1.43	27.03	1.62	47.84	1.87	78.55

The results presented in Table 1 show that the saturation of MRF122-2ED, MRF132-AD, and MRF241-ES fluids occurred at about 1.0, 1.23, and 1.49 Tesla, respectively. Furthermore, these fluids seem to be able to provide maximum yield stresses of about 27, 48, and 78 kPa, respectively.

The MR fluid gap size h was fixed at 2 mm, which is similar to fluid gaps set in previous designs of various MR fluid devices (see for example El Wahed and McEwan, 2011; El Wahed and Balkhoyor, 2015, 2016). Also, the fluid temperature was assumed to be maintained at 40 °C at which the viscosity, η for MRF122-2ED, MRF132-AD, and MRF241-ES fluids was set to 70, 90 and 88 mPa.s, respectively (Lord Corporation, 2008). According to the optimized design of the ball-and-socket actuator (Almazroa, 2011), the socket opening angle, φ (from one socket edge to another) and the radius, r of the actuator ball are set to 125° and 50 mm, respectively. In addition, an angular velocity, ω of 1 rad/s is considered in this investigation. Considering the estimated yield stress, τ (H) values provided by the employed fluids (Table 1) and the corresponding magnetic flux densities, B, equation (11) was used to estimate the torques delivered by the ball-and-socket actuator and the results will be presented and compared with the numerical results later in Section 4 for the three commercial fluids.

4. CFD SIMULATION OF THE DEVICE TRANSMITTED TORQUE

Based on a socket angle of opening, φ of 125° and an MR fluid gap thickness of 2.0 mm, a fluid volume was created into the ANSYS CFX environment which takes the shape shown in Figure 6.

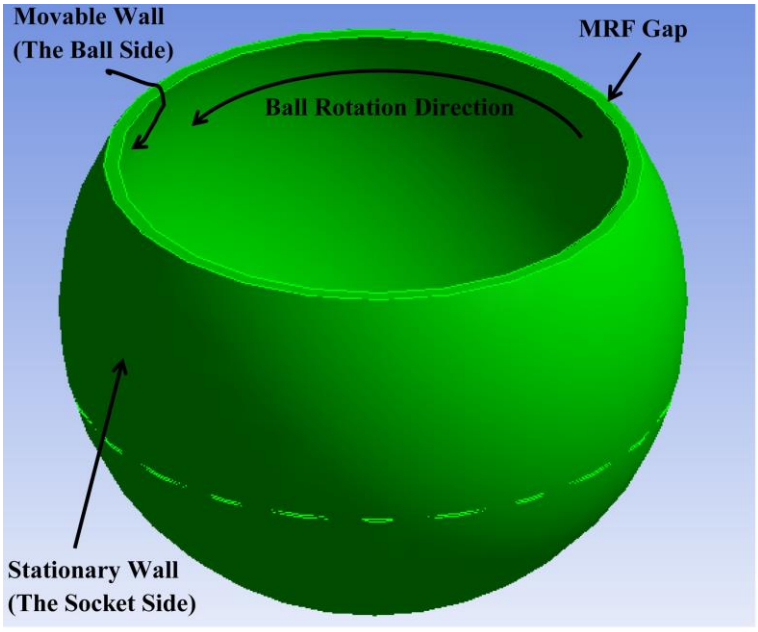

Figure 6. MR fluid volume between the ball and socket components

It is assumed that the electromagnetic circuit of the actuator generates a uniformly distributed magnetic flux along the MR fluid gap and therefore, the yield stress of the MR fluid is considered to be constant throughout the fluid volume. In the present investigation, equation (12) was used to provide yield stress values into ANSYS CFX depending on the magnetic field intensity, which is related to the flux density through equation (13). These data are already presented in Table 1.

As it was mentioned earlier, the fluid temperature was assumed to be maintained at 40 °C for which the density for MRF122-2ED, MRF132-AD, and MRF241-ES fluids was set in these CFD simulations to 2380, 3090 and 3860 kg/m^3, respectively (Lord Corporation, 2008).

The socket surface in contact with the MR fluid was considered to be a stationary wall, which was represented in the CFX code by the non-slip velocity condition. This boundary condition is usually achieved when the three velocity components in the three coordinate directions are set to zero. However, the ball was subjected to an angular speed and hence, its surface that is in contact with the MR fluid was considered to be a moving wall. In the current CFX simulation, the ball was assumed to rotate about the y-axis (see Figure 6) with an angular speed set to 1 rad/s. The top horizontal surface of the fluid at the socket opening was considered as a stationary wall (no-slip condition) since it is in contact with a large lip-seal blocking the MR fluid gap.

For low angular speeds, the MR fluid flow inside the gap initiated by the ball motion was assumed to be steady, laminar, and incompressible. In addition, thermal interaction inside the MR fluid was ignored and therefore, the flow was assumed to be under adiabatic conditions. The minimum pressure magnitude was also assumed to be above the fluid vapour pressure so that any cavitation was excluded from the analysis.

The CFD analysis was repeated for the three commercial MR fluids and the results are presented in terms of the fluid shear stress as a function of the magnetic flux density. In addition, the performance of the actuator was assessed when the torque transmitted by the MR fluid was determined under the above conditions. Figure 7 shows a flowchart summarizing the solution steps.

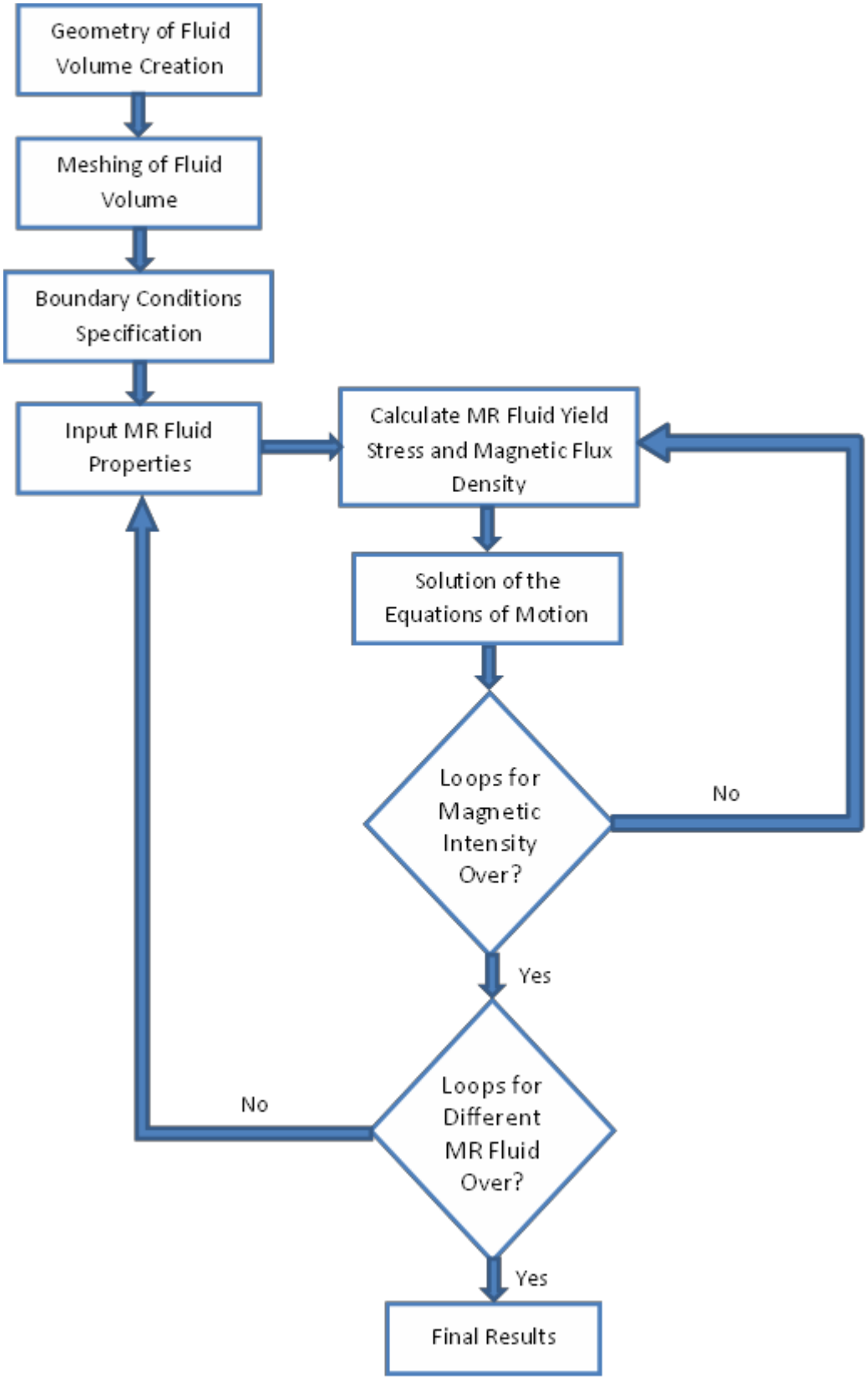

Figure 7. Flowchart of CFD simulation procedure

It is well known that CFD solutions are dependent on the mesh type and density. The thin MR fluid volume formed between the actuator ball and socket should be well described, with a relatively dense mesh. In this investigation, trial and error technique was applied to determine the optimum mesh for the MR fluid volume. Figure 8 shows the meshed fluid volume with a minimum element size of 3.5×10^{-4} m.

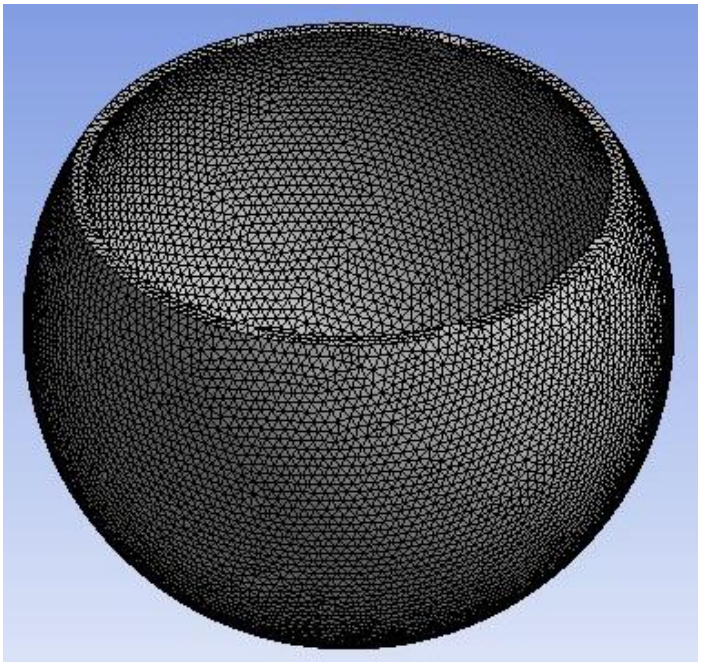

Figure 8. Mesh of the MR fluid volume model

The MR fluid properties including density and viscosity together with the estimated yield stress values (Table 1) were then input in the CFX programme. This should make the model ready to be solved for the aimed yield stress magnitude and hence the magnetic field excitation level, which when completed, the results could be presented into various forms. The procedure was repeated for the remaining yield stress magnitudes (Table 1). The same steps were then repeated for the other MR fluids used in this investigation.

Figure 9 shows an isometric view of the MRF132-AD fluid velocity in the fluid gap between the ball and socket components of the actuator for the Newtonian case, when the current supplied to the coil was assumed to be zero. It can be seen that the velocity on the outer surface of the fluid volume, which is in contact with the socket surface, is zero whilst the maximum velocity is seen to occur on the fluid side that is in contact with the moving ball. This velocity also seems to decrease from the maximum value which occurs near by the socket opening to the lowest value that is estimated in areas close to the bottom end (the centre) of the socket where the fluid is deemed to be stationary.

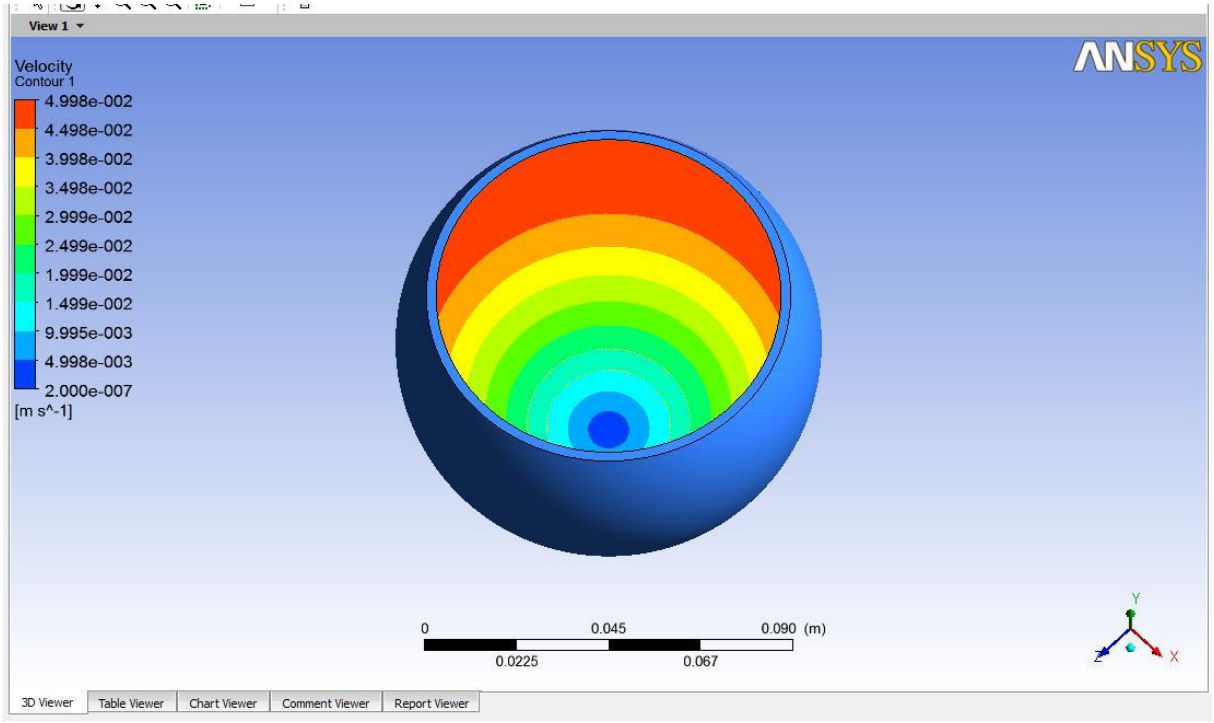

Figure 9. Isometric view of the velocity contour along the MRF132-AD fluid volume

In addition, the top fluid surface at the socket opening was considered as a stationary surface under no-slip boundary condition and hence, the velocity appears to increase from zero at this surface to a maximum value along the fluid surface adjacent to the ball, as shown in Figure 10.

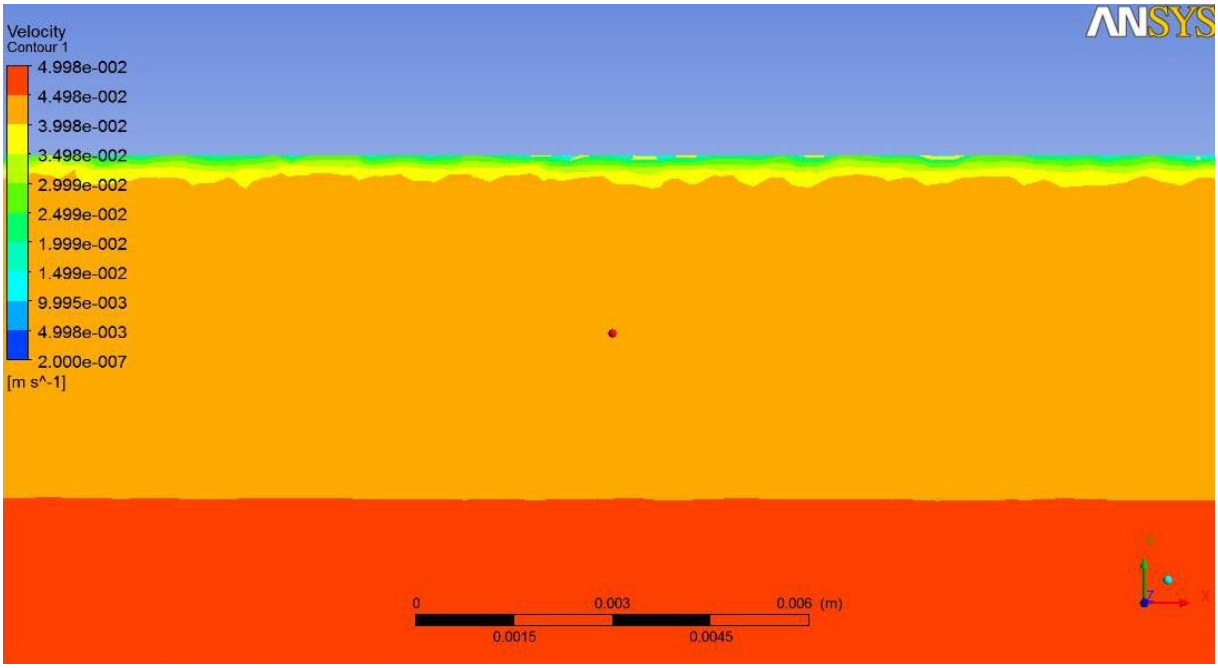

Figure 10. Boundary layer development along the MRF132-AD fluid surface adjacent to the ball surface starting from the top fluid stationary surface

Figure 11 shows the wall shear stress distribution for the Newtonian fluid case of MRF132-AD fluid. It can be seen that the wall shear stress increases from the minimum magnitude, which occurs in areas close to the bottom side of the socket, around its centerline, to the maximum that occurs in areas close to the socket opening. This could be ascribed to the fact that the moment arm (r . sin φ), which is multiplied by the shearing force to obtain the torque, becomes larger when the angle of the socket opening, φ, increases from zero at the centre of the socket to 90 degrees near by the socket opening (see section 3).

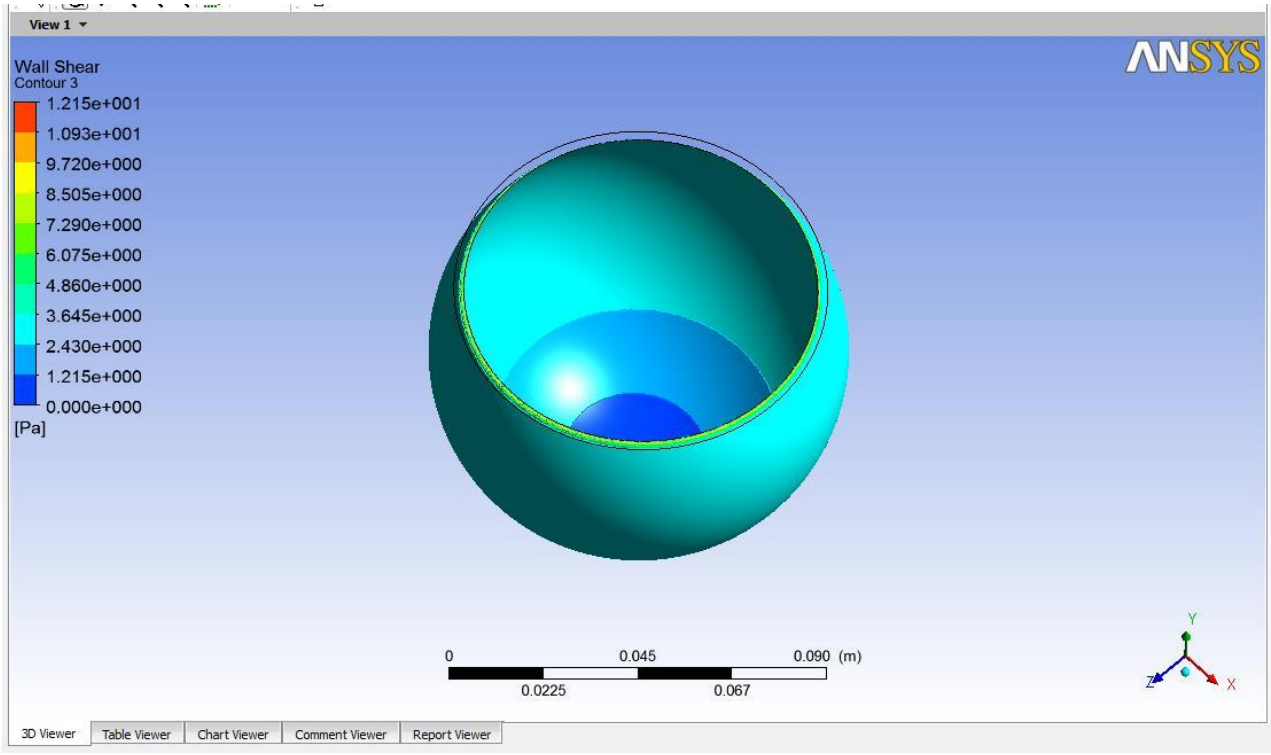

Figure 11. Shear stress distribution on the MRF132-AD fluid volume

The shear stress was then estimated for various magnetic field densities, namely in the range between 0 and 1.5 Tesla and the results are shown in Figure 12 for the three investigated MR fluids. It is interesting to observe that the behavior of the water-based MRF241-ES fluid is different to those exhibited by the other oil-based fluids, particularly at the lower end of the magnetic excitation range. It can also be seen that fluids with higher solid-phase volume fraction deliver higher shear stress, which is due to the fact that fibrillation becomes stronger with higher particulate concentration (El Wahed, 2011).

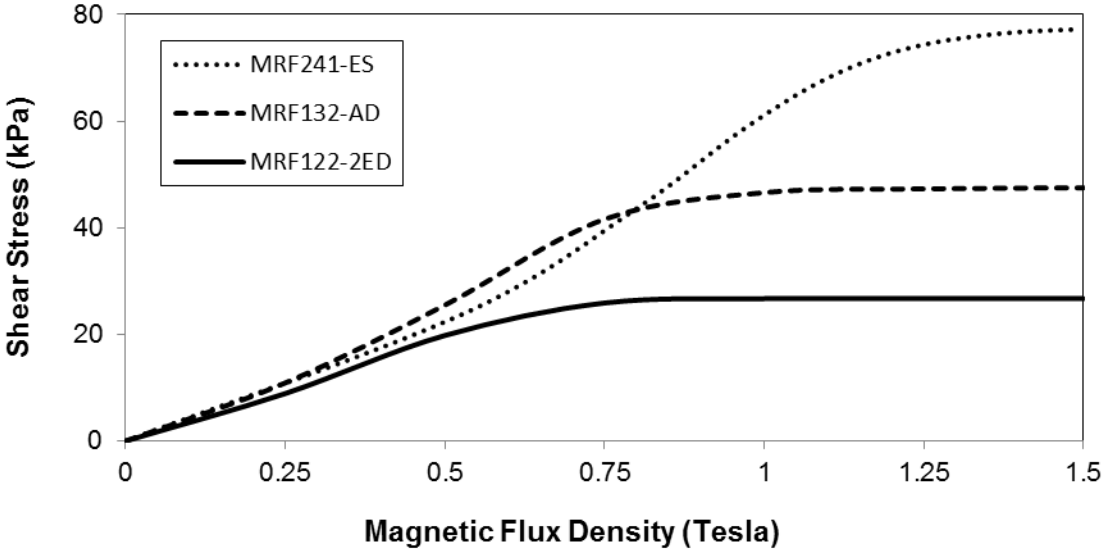

Figure 12. Shear stress versus magnetic flux density for three commercial MR fluids

ANSYS CFX was used to estimate the torque transmitted by the MR fluid to the socket surface as a result of the ball actuation (angular speed of 1 rad/s). Figure 13 shows the torque results as a function of the magnetic flux density for the three investigated MR fluids. It can be seen that the transmitted torque increases with the magnetic flux density reaching asymptotic values of about 28, 49 and 81 N.m for MRF122-2ED, MRF132-AD, and MRF241-ES fluids, respectively when the fluids were excited by about 1.1, 1.3 and 1.5 Tesla, respectively indicating that the fluids become magnetically saturated at this magnetic excitation level. It is clear that MRF241-ES fluid was cable to supply higher actuator performance in comparison with those provided by MRF122-2ED and MRF132-AD fluids due to its high yield stress functionality.

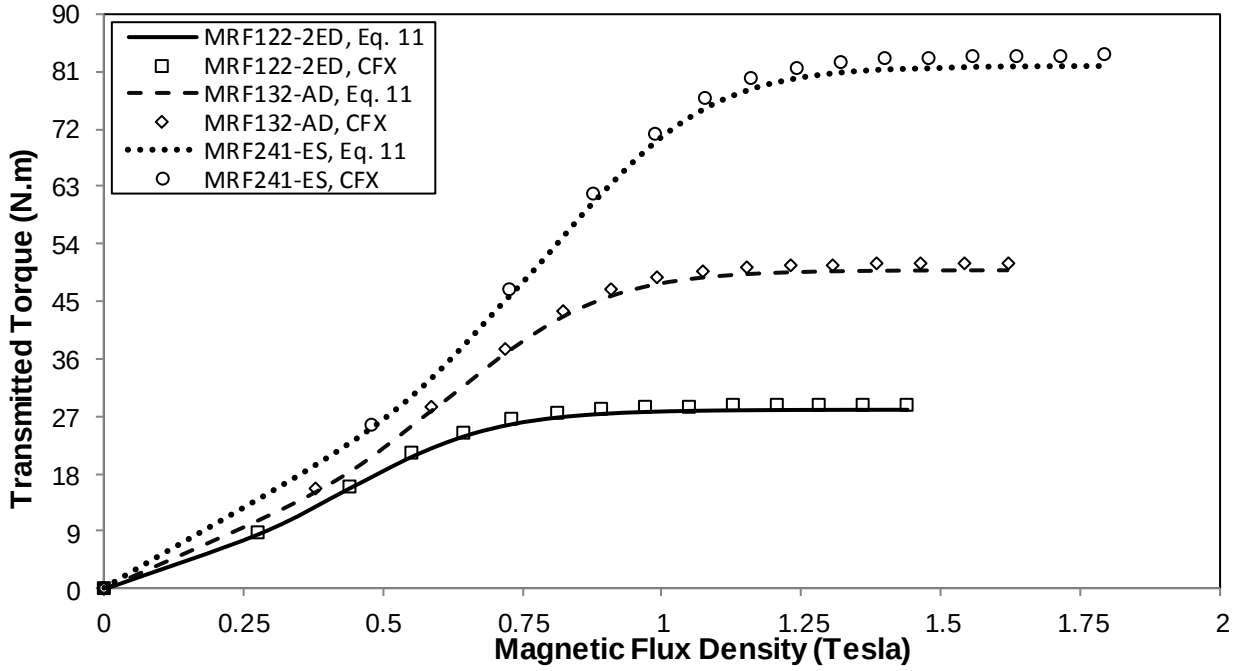

Figure 13. Torque transmitted versus magnetic flux density for three commercial fluids

The torque transmitted by the ball-and-socket actuator was also theoretically estimated using equation 11 and the results are also shown in Figure 13 for the three investigated MR fluids. It can be seen that there is a good agreement between the numerical and the theoretical results. This concludes that the CFD technique, which has been successfully applied in this investigation to estimate the ball-and-socket actuator performance, could be used as a cost-effective technique to determine the performance of other smart fluid devices such as clutches, brakes, and dampers.

5. CONCLUSIONS

This article has been concerned with an assessment of the comparative performance of a smart ball-and-socket actuator employing MR fluids using theoretical and numerical approaches. The theoretical model combines the viscous-friction and the controllable field-dependent characteristics of the MR fluid whilst the numerical results were achieved using computational fluid dynamics (CFD) technique which was carried out using ANSYS CFX computer code. Three commercial MR fluids manufactured by Lord Corporation were used in this investigation. The main aim was to quantify the torque capability of the smart actuator and both modelling techniques produced closely-matched results, which were found to be adequate for human upper-limb rehabilitation applications.

The CFD technique employed in this investigation to estimate the performance of the smart ball-and-socket actuator has been proven to be an accurate and a cost-effective technique, which could be applied to assess the performance of other smart actuators.

ACKNOWLEDGEMENT

This research received no specific grant from any funding agency in the public, commercial, or not- for-profit sectors.

REFERENCES

Abrams W and Berkow R (1997) Merk Manual of Geriatrics, Merk Research Laboratories, Whitehouse Station, New Jersey.

Alexander MA, Nelson MR and Shah A (1992) Orthotics, adapted seating and assistive devices. In: Pediatric Rehabilitation, 2nd ed. Baltimore, MD: Williams and Wilkins, pp. 186–187.

Almazroa A (2011) Smart actuators and their application into rehabilitation training systems. MPhil Thesis, University of Dundee, UK.

Anon, 1995, Brake cuts exercise equipment cost. Design News, 39: 4.

Arre Industries, (1998) Carrera MagneShock, 5412, New Peachtree St, Atlanta, GA.

Baklouti M, AbouSaleh J, Monacelli E and Couvet S (2010) Human Machine Interface in Assistive Robotics: Application to a Force Controlled Upper-Limb Powered Exoskeleton. In: Abdellatif H (ed) Robotics 2010 Current and Future Challenges. Rijeka, Croatia: InTech, pp. 211-223.

Benjuya N and Kenney SB (1990) Hybrid arm orthosis. Journal of Prosthetics and Orthotics 2(2): 155–163.

Burgar CG, Lum PS, Shor PC and Machiel Van der Loos HF (2000) Development of robots for rehabilitation therapy: The Palo Alto VA/Stanford experience. Journal of Rehabilitation Research and Development 37(6): 663-673.

Carlson JD, Matthis W and Toscano JR (2001) Smart prosthetics based on magnetorheological fluids. Proceedings of SPIE 4332: 308-316.

Claas Tractor Times, Spring 2008.

Delphi Energy & Chassis Systems, 2002, Pub. DE-00-E-019.

Dickerson CR, Martin BJ and Chaffin DB (2006) The relationship between shoulder torques and the perception of muscular effort in loaded reaches. *Ergonomics* 49(11): 1036–1051.

Dijkers MP, deBear PC, Erlandson RF, Kristy K, Geer DM and Nichols A (1991) Patient and staff acceptance of robot technology in occupational therapy: A pilot study. Journal of Rehabilitation Research and Development 28(2): 33–44.

Dong S, Lu KQ, Sun JQ and Rudolph K (2006) Adaptive force regulation of muscle strengthening rehabilitation device with magnetorheological fluids. IEEE Transactions on Neural Systems and Rehabilitation Engineering 14(1): 55-63.

Dundee Healthcare NHS Trust, Out-patient Continuum Physiotherapy Database, 1992-1997.

El Wahed AK (2011) The influence of solid-phase concentration on the performance of electrorheological fluids in dynamic squeeze flow. Materials Design 32: 1420–1426.

El Wahed AK and McEwan CA (2011) Design and Performance Evaluation of Magnetorheological Fluids under Single and Mixed Modes. *Journal of Intelligent Material Systems and Structures* 22: 631-643.

El Wahed AK and Balkhoyor LB (2015) Magnetorheological fluids subjected to tension, compression, and oscillatory squeeze input. *Smart Structures and Systems* 16(5): 961-980.

El Wahed AK and Balkhoyor LB (2016) Characteristics of magnetorheological fluids under single and mixed modes. Proceedings of the Institution of Mechanical Engineers, Part C: Journal of Mechanical Engineering Science 231(20): pp. 3798-3809.

Feys HM De Weerdt WJ and Selz BE (1998) Effect of therapeutic intervention for the hemiplegic upper limb in the acute phase after stroke: a single-blind, randomised, controlled multi-centre trial. Stroke 29: 785-792.

Furusho J, Kikuchi T and Oda K (2002) Isokinetic exercise training and evaluation system using particle-type ER fluid. Transactions of the Japan Society of Mechanical Engineers, Part C 68(8): 2418-2424.

Furusho J, Li C, Hu X, Shichi N, Kikuchi T, Inoue A, Nakayama K, Yamaguchi Y and Ryu U (2006) Development of a 6-DOF force display system using ER actuators with high-safety. Proceedings - VRCIA 2006ACM International Conference on Virtual Reality Continuum and its Applications: 405-408.

Hakogi H, Ohaba M, Kuramochi N and Yano H (2006) Torque control of a rehabilitation teaching robot using magneto-rheological fluid clutches. JSME International Journal, Series B: Fluids and Thermal Engineering 48(3): 501-507.

Hawkins P, Smith J, Alcock S, Topping M, Harwin W, Loureiro R, Amirabdollahian F, Brooker J, Coote S, Stokes E, Johnson G, Mak P, Collin C and Driessen B (2002), GENTLE/S Project: Design and Ergonomics of a Stroke Rehabilitation System. In: Proceedings of 1st Cambridge Workshop on Universal Access and Assistive Technology (CWUAAT) (incorporating 4th Cambridge Workshop on Rehabilitation Robotics) Published by University of Cambridge, Cambridge UK, 25–27 March 2002, pp. 85-90.

Homma K and Arai T (1995) Design of an upper limb assist system with parallel mechanism. In: The 1995 IEEE International Conference on Robotics and Automation, Nagoya, Aichi, Japan, 21-27 May 1995, pp. 1302–1307.

Hwang YH, Kang SR, Cha SW and Choi SB (2016) An electrorheological spherical joint actuator for a haptic master with application to robot-assisted cutting surgery. Sensors & Actuators, A-Physical 249: 163-171.

Jaffar AA, Abass SJ and Ismael MQ (2006) Biomechanical Aspects of Shoulder and Hip Articulations: A Comparison of Two Ball and Socket Joints. Al-Khwarizmi Engineering Journal 2(1): 1-14.

Johnson GR and Buckley MA (1997) Development of a new Motorised Upper Limb Orthotic System (MULOS). In: Proceedings of the Rehabilitation Engineering Society of North America, (ed S Springle), Pittsburgh, PA, 20-24 June 1997, pp. 399–401. RESNA Press.

Kavlicoglu BM, Gordaninejad F, Evrensel CA, Liu V, Kavlicoglu N and Fuchs A (2008) Heating of a high-torque magnetorheological fluid limited slip differential clutch. Journal of Intelligent Material Systems and Structures 19: 235-241.

Khanicheh A, Mintzopoulos D, Weinberg B, Tzika AA and Mavroidis C (2008) MR_CHIROD v.2: Magnetic resonance compatible smart hand rehabilitation device for brain imaging. IEEE Transactions on Neural Systems and Rehabilitation Engineering 16(1): 91-98.

Kikuchi T, Ozawa T, Akai H and Furusho J (2009) Hybrid-PLEMO, rehabilitation system for upper limbs with active / passive force feedback, and its application for facilitation techniques. 2009 IEEE International Conference on Rehabilitation Robotics, ICORR 2009, Article. no. 5209594: 781-786.

Krebs HI, Hogan N, Aisen ML and Volpe BT (1998) Robot-aided neurorehabilitation. IEEE Transactions on Rehabilitation Engineering 6(1): 75-87.

Lee KM, Roth RB and Zhou Z (1996) Dynamic modelling and control of a ball-joint-like variable-reluctance spherical motor. Journal of Dynamic Systems, Measurement and Control 118(1): 29-40.

Lincoln NB, Parry RH and Vass CD (1999) Randomised, controlled trial to evaluate increased intensity of physiotherapy treatment of arm function after stroke. Stroke 30: 573-579.

Linde, 2000, Lansing Linde Ltd., U.K.

LORD MR Fluids Technical Summary, Lord Corporation, www.lordfulfillment.com, 2008.

McManus SJ and St Clair KA (2000) Ergonomics, work station and driver issues. SAE Technical Paper Series, Paper No. 2000-01-3408, Truck and Bus Meeting and Exposition.

Nef T, Guidali M and Riener R (2009) ARMin III - Arm therapy exoskeleton with an ergonomic shoulder actuation. Applied Bionics and Biomechanics 6: 127-142.

Nguyen QH, Nguyen ND and Choi SB (2015) Design and evaluation of a novel magnetorheological brake with coils placed on the side housings. Smart Materials and Structures 24(4): 1-12.

Nikitczuk J, Weinberg B and Mavroidis C (2007) Control of electro-rheological fluid based resistive torque elements for use in active rehabilitation devices. Smart Materials and Structures 16(2): 418-428.

Parker VM, Wade DT and Langton-Hewer R (1986) Loss of arm function after stroke: Measurement, frequency, and recovery. International Rehabilitation Medicine 8: 69-73.

Peters D, Davies and Pietroni P (1994) Musculoskeletal clinic in general practice: study of one year's referrals. British Journal of General Practice 44(378): 25–29.

Peterson S, Rayner M and Press V (2000) Coronary Heart Disease Statistics, 2000 Edition, The British Heart Foundation Statistics Database.

Powell J, Pandyan AD, Granat M, Cameron M and Stott DJ (1999) Electrical stimulation of wrist extensors in poststroke hemiplegia. Stroke 30: 1384-1389.

Reinkensmeyer DJ, Dewald JPA and Rymer WZ (1999) Guidance-based quadification of arm impairment following brain injury. IEEE Transactions on Rehabilitation Engineering 7(1): 1-11.

Sakaguchi M, Furusho J and Genda E (1999) Basic study on rehabilitation training system using ER actuators. Proceedings of the IEEE International Conference on Systems, Man and Cybernetics l(1): 135-140.

Senkal D and Gurocak H (2009) Spherical brake with MR fluid as multi degree of freedom actuator for haptics. Journal of Intelligent Material Systems and Structures 20: 2149-2160.

Shames IH and Cozzarelli FA (1992) Elastic and Inelastic Stress Analysis. Englewood Cliffs, NJ: Prentice-Hall.

Stern PH and Lauko T (1975) Modular designed wheelchair based orthotic system for upper extremeties. Paraplegia 12: 299–304.

The Chartered Society of Physiotherapy, Information Department, March 1998.

Trivedi V (2009) Smart actuators for rehabilitation training systems. MSc Thesis, University of Dundee, UK.

Tsagarakis NG and Caldwell DG (2003) Development and control of a soft-actuated exoskeleton for use in physiotherapy and training. Autonomous Robots 15: 21-33.

Zite JL, Ahmadkhanlou F, Neelakantan VA and Washington GN (2006) A magnetorheological fluid based orthopedic active knee brace. Proceedings of SPIE - The International Society for Optical Engineering 6171, Article no. 61710H.